12-2001

Discrete Singular Convolution for the Prediction of High Frequency Vibration of Plates

Yibao ZHAO
Singapore Management University, ybzhao@smu.edu.sg

G. W. WEI
National University of Singapore

Y. XIANG
University of Western Sydney
DOI: https://doi.org/10.1016/s0020-7683(01)00183-4

Published in International Journal of Solids and Structures, Volume 39, Issue 1, December 2001, Pages 65-88
https://doi.org/10.1016/s0020-7683(01)00183-4

Discrete singular convolution for the prediction of high frequency vibration of plates

Y.B. Zhao [a], G.W. Wei [a,*], Y. Xiang [b]

[a] *Department of Computational Science, National University of Singapore, Block S17, Level 7, 3 Science Drive, Singapore 117543, Singapore*

[b] *School of Engineering and Industrial Design, University of Western Sydney, Penrith South DC, NSW 1797, Australia*

Abstract

Theoretical analysis of high frequency vibrations is indispensable in a variety of engineering designs. Much effort has been made on this subject in the past few decades. However, there is no single technique which can be applied with confidence to various engineering structures for high frequency predictions at present. This paper introduces a novel computational approach, the discrete singular convolution (DSC) algorithm, for high frequency vibration analysis of plate structures. Square plates with six distinct boundary conditions are considered. To validate the proposed method, a completely independent approach, the Levy method, is employed to provide exact solutions for a comparison. The proposed method is also validated by convergence studies. We demonstrate the ability of the DSC algorithm for high frequency vibration analysis by providing extremely accurate frequency parameters for plates vibrating in the first 5000 modes.

Keywords: Plates; High order modes; High frequency vibration; Wavelets; Discrete singular convolution

1. Introduction

In modern industry and scientific applications, both ordered and random high frequency motions are frequently encountered. For example, the frequency of magic angle spin in a solid nuclear magnetic resonance spectroscopy is about 40 kHz. The turbulence combustion field of a space shutter or a jet fighter engine contains very high frequency (color) noise components. As a result, many man-made structures, such as aircraft, jet, satellite, computer hard disc, and mobile phone are subjected to various high frequency excitations. To avoid mechanical resonance and fatigue damage in engineering designs, it is crucial to predict and understand the mechanical responses of a man-made structure subject to high frequency vibration and noise. The most commonly used approaches of high frequency analysis include hierarchical finite element method (HFEM) (Langley and Bardell, 1998), dynamic stiffness (continuous element) method

* Corresponding author. Tel.: +65-874-6589; fax: +65-774-6756.
E-mail address: cscweigw@nus.edu.sg (G.W. Wei).

(Wang and Kinsman, 1971; Banerjee and Williams, 1994), Levy method (Xiang et al., 1996), periodic structure approximation (Mester and Benaroya, 1995; Mead, 1996), statistical energy analysis (Lyon, 1975; Keane and Price, 1987) and wave intensity analysis (Langley and Khumbah, 1995). Among these methods, the last three approaches treat the original physical system in a manner which might not necessarily be the same as the exact mechanical analysis. For example, periodic structure theory assumes an idealized periodicity which is indeed very efficient for handling many real-world structures. Statistical energy analysis does not attempt to predict detailed high frequency modes. Instead, it provides the spatial frequency distribution of a structure. Such information is valuable for estimating the frequency response of a structure under external noise. As a generalization of the statistical energy analysis, wave intensity analysis does not assume a diffusive vibration wave field. In contrast, other three approaches, i.e., the HFEM, dynamic stiffness method and Levy method, attempt to solve the original integral equations and/or differential equations which are derived from the established principles of applied mechanics. In particular, dynamical stiffness method has been extensively used for one-dimensional structural analysis with success. When applied to a complex two-dimensional structure, the method essentially treats an idealized structure. The Levy method is capable of providing closed-form solutions for rectangular plates that have at least two parallel edges simply supported. The full solution of arbitrary accuracy can be obtained by sufficient number of iterations. Recently, Beslin and Nicolas proposed an HFEM (Beslin and Nicolas, 1997) to reduce the well-known numerical instability of the conventional p-version finite element method due to computer's round-off errors. The p-version finite element method utilizes a degree p of the basis functions which are conventionally chosen either as polynomial sets such as integrated Legendre polynomials, Jacobi polynomials, or as the Taylor basis $\{x^n\}$. For a relatively large p, the high numerical dynamics of these polynomial coefficients causes computer's round-off errors and leads to ill-conditioned mass and stiffness matrices. The HFEM proposed by Beslin and Nicolas uses a trigonometric set $\{\phi(x)\}$ of the form

$$\phi_r(x) = \sin(a_r x + b_r)\sin(c_r x + d_r), \quad r = 1, 2, \ldots \tag{1}$$

as basis functions. Here coefficients a_r, b_r, c_r and d_r are chosen appropriately (Beslin and Nicolas, 1997) to satisfy the boundary conditions of a plate. Remarkably, such an HFEM works much better than the hierarchical FEM of Bardell (1991) for high frequency analysis and was devised to predict the 850th mode for an all edge simply supported rectangular plate and the 820th mode for an all edge free plate with errors being less than 2%. However, due to numerical instability, it is still very difficult for the HFEM to pursue beyond vibration modes of the order of a thousand (Beslin and Nicolas, 1997). Moreover, the accuracy of the HFEM for lower modes is quite low. Therefore, despite much effort in the past few decades, unfortunately, there is no single technique which can be applied with confidence to high frequency vibration analysis (Langley and Bardell, 1998) at present. The reader is referred to Langley and Bardell (1998) for an elegant review on this subject.

More recently, the discrete singular convolution (DSC) algorithm (Wei, 1999a, 2000a,b) has emerged as a potential approach for the computer realization of singular integrations. Sequences of approximations to the singular kernels of Hilbert type, Abel type and delta type were constructed. The mathematical foundation of the DSC algorithm is the theory of distributions (Schwartz, 1951) and the theory of wavelets. Numerical solutions to differential equations are formulated via the singular kernels of delta type. For the purpose of numerical computations, both *bandlimited reproducing kernels* and *approximate reproducing kernels* are discussed as sequences of approximations to the *universal reproducing kernel*, the delta distribution. By appropriately selecting parameters in a DSC kernel, the DSC approach exhibits controllable accuracy for integration and shows excellent flexibility in handling complex geometries and boundary conditions. It was demonstrated (Wei, 2000a) that different implementations of the DSC algorithm, such as global, local, Galerkin, collocation, and finite difference, can be deduced from a single starting point. Thus, the DSC algorithm provides a unified representation to these numerical methods. Practical applications

were examined for the numerical solution of the Fokker–Planck equation (Wei, 1999a, 2000a) and for the Schrödinger equation (Wei, 2000c). Another development in the application of the DSC algorithm is its use in computing numerical solutions of the Navier–Stokes equation with both regular (Wei, 2001a) and irregular geometries (Wan et al., in press). In the context of image processing, DSC kernels were used to facilitate a new anisotropic diffusion operator for image restoration from noise (Wei, 1999b). Most recently, the DSC algorithm was used to integrate the Cahn–Hilliard equation in a circular domain (Guan et al., 2001) and the sine-Gordon equation with the initial values close to a homoclinic manifold singularity (Wei, 2000d), for which conventional local methods encounter great difficulties and result in numerically induced chaos (Ablowitz et al., 1996). The work most relevant to the present study is the use of DSC for plate (Wei, 1999c, 2001b) and beam (Wei, 2001c) analyses. The DSC algorithm was utilized to provide the first 100 modes of a simply supported square plate with at least 11 significant figures (Wei, 1999c, 2001b). We illustrated that the DSC provides excellent results for plates with internal line supports (Wei et al., in press), complex internal supports (Xiang et al., in press) and irregular internal supports (Zhao et al., in press).

The objective of the present paper is to introduce the DSC algorithm for high frequency vibration analysis of plates. To validate the present DSC results, closed-form solutions are generated by using a completely independent approach, the Levy method, for cross-validations. The validity and accuracy of the DSC method for higher-mode vibration analysis of plates are verified by convergence studies and a comparison with the Levy solutions. Extensive frequency parameters are tabulated for square plates of six distinct edge support conditions obtained as a combination of simply supported and clamped edges. We demonstrate that the DSC approach is able to provide extremely accurate vibration modes of the order of a few thousands without encountering any difficulty of numerical instability. In fact, the true potential of the DSC algorithm for the prediction of high frequency vibration is unknown to us at the moment. It seems to be limited only by computer memory and CPU time.

The organization of the paper is as follows. Theory and algorithm for plate analysis are given in Section 2. For the sake of integrity, we briefly review the computational philosophy of the DSC algorithm and the Levy method. Numerical experiments are presented in Section 3 by using both the DSC and Levy methods. Case studies are performed on various combinations of different boundary conditions. This paper ends with a conclusion.

2. Theory and algorithm

The problem of plate vibration with different boundary conditions is described. For integrity and convenience, both the DSC and Levy methods are briefly reviewed in this section. However, the reader is referred to the original work for more details (Wei, 1999a). The analysis of plates by both methods is presented.

2.1. Theory of plates

Although we limit our attention to the vibration of rectangular (classic) Kirchhoff plates with simply supported and clamped edges, the method can be used for many other applications in solid mechanics. Let us consider a rectangular plate of length a, width b, thickness h, mass density ρ, modulus of elasticity E, and Poisson's ratio v. The origin of the Cartesian coordinates (x, y) is set at the lower left corner of the plate. The governing differential equation for the plate is given by (Timoshenko and Woinowsky-Krieger, 1970)

$$\frac{\partial^4 w}{\partial x^4} + 2\frac{\partial^4 w}{\partial x^2 \partial y^2} + \frac{\partial^4 w}{\partial y^4} = \frac{\rho h \omega^2}{D} w, \tag{2}$$

where $w(x,y)$ is the transverse displacement of the midsurface of the plate, $D = Eh^3/[12(1-v^2)]$ the flexural rigidity, and ω the circular frequency. We consider one of the following two types of support conditions for each plate edge:

For simply supported edge (S):

$$w = 0, \quad -D\left(\frac{\partial^2 w}{\partial n^2} + v\frac{\partial^2 w}{\partial s^2}\right) = 0. \tag{3}$$

For clamped edge (C):

$$w = 0, \quad \frac{\partial w}{\partial n} = 0, \tag{4}$$

where n and s denote, respectively, the normal and tangential coordinates with respect to the considered edge.

It is pointed out that the thin plate theory used in this study may not be strictly valid in predicting the very high frequency vibration of real plates. In particular, if a plate vibrates in very high frequency, the wavelength of a vibration mode may be comparable to or even smaller than the thickness dimension of the plate. In such a case, rotary inertia and transverse shear deformation may have significant influence on the vibration behavior of the plate. A better approximation can be achieved by employing either the first-order plate theory (the Mindlin plate theory (Mindlin, 1951)), the higher-order plate theory (the Reddy plate theory (Reddy, 1984)) or the three-dimensional (3D) theory for elasticity. Nevertheless, the objective of this paper is to demonstrate the ability of the DSC algorithm in dealing with high frequency vibrations. It is believed that the DSC approach for high frequency analysis introduced in the present work can be easily adopted for solving problems based on other structural theories.

It is well known that high frequency vibrations are very sensitive to boundary conditions, structural geometries, and geometrical and material imperfections. The treatment of different boundary conditions are presented in the present study. The use of the DSC algorithm for complex geometries is studied for incompressible flow (Wan et al., in press) and is under consideration for structural analysis. The geometrical and material imperfections might be modeled by improved plate theories, whose governing equations can be solved similarly by using the proposed DSC algorithm.

2.2. Discrete singular convolution

Singular convolutions are essential to many science and engineering problems, such as electromagnetics, Hilbert transform, Abel and Radon transforms. DSC is a general approach for the numerical realization of singular convolutions. By appropriate construction or approximation of a singular kernel, the DSC can be an extremely efficient, accurate and reliable algorithm for practical applications (Wei, 1999a).

It is very convenient to discuss singular convolution in the context of distributions. We denote T a distribution and $\eta(t)$ an element of the space of test functions. A singular convolution can be expressed as

$$F(t) = \int_{-\infty}^{\infty} T(t-x)\eta(x)\,\mathrm{d}x. \tag{5}$$

Here $T(t-x)$ is a singular kernel. Depending on the form of the kernel T, the singular convolution is the central issue for many science and engineering problems. For example, singular kernels of the Hilbert type have a general form of

$$T(x) = \frac{1}{x^n} \quad (n > 0). \tag{6}$$

Here, kernels $T(x) = 1/x^a$ $(0 < a < 1)$ define the Abel transform which is closely connected with a generalization of the tautochrone problem. Kernel $T(x) = 1/x$ commonly occurs in theory of linear response,

signal processing, theory of analytic functions, and the Hilbert transform. Its 3D version is important to the theory of electromagnetics. $T(x) = 1/x^2$ is the kernel used in tomography. Other interesting examples are singular kernels of the delta type

$$T(x) = \delta^{(n)}(x) \quad (n = 0, 1, 2, \ldots). \tag{7}$$

Here, kernel $T(x) = \delta(x)$ is important for interpolation of surfaces and curves; and $T(x) = \delta^{(n)}(x)$ $(n = 1, 2, \ldots)$ are essential for numerically solving differential equations. However, a common feature of these kernels is that they are singular, i.e. they cannot be directly digitized in computers. In this regard, the singular convolution, Eq. (5), is of little numerical merit. To avoid the difficulty of using singular expressions directly in computers, sequences of approximations (T_α) of the distribution T can be constructed

$$\lim_{\alpha \to \alpha_0} T_\alpha(x) \to T(x), \tag{8}$$

where α_0 is a generalized limit. Obviously, in the case of $T(x) = \delta(x)$, the sequence, $T_\alpha(x)$, is a delta sequence. Furthermore, with a good approximation, it makes sense to consider a *discrete* version

$$F_\alpha(t) = \sum_k T_\alpha(t - x_k) f(x_k), \tag{9}$$

where $F_\alpha(t)$ is an approximation to $F(t)$ and $\{x_k\}$ is an appropriate set of discrete points on which the discrete convolution (9) is well defined. It is this discrete expression that makes a computer realization possible. Note that, the original test function $\eta(x)$ has been replaced by $f(x)$. The mathematical property or requirement of $f(x)$ is determined by the approximate kernel T_α. In general, the convolution is required being Lebesgue integrable.

It is helpful to illustrate the algorithm by examples. A simple example is Shannon's wavelet kernel, $\sin \alpha x / \pi x$. Shannon's wavelet kernels are a delta sequence and thus provide an approximation to the delta distribution

$$\lim_{\alpha \to \infty} \left\langle \frac{\sin \alpha x}{\pi x}, \eta(x) \right\rangle = \eta(0). \tag{10}$$

Other important examples include the Dirichlet kernel

$$\frac{\sin\left[\left(l + \frac{1}{2}\right)(x - x')\right]}{2\pi \sin\left[\frac{1}{2}(x - x')\right]}, \tag{11}$$

the modified Dirichlet kernel

$$\frac{\sin\left[\left(l + \frac{1}{2}\right)(x - x')\right]}{2\pi \tan\left[\frac{1}{2}(x - x')\right]} \tag{12}$$

and the de la Vallée Poussin kernel

$$\frac{1}{\pi\alpha} \frac{\cos[\alpha(x - x')] - \cos[2\alpha(x - x')]}{(x - x')^2}. \tag{13}$$

For sequences of the delta type, an interpolating (or quasi-interpolating) algorithm sampling at Nyquist frequency, $\alpha = \pi/\Delta$, has great advantage over a non-interpolating discretization. Therefore, the Shannon's wavelet kernel is discretized as

$$\frac{\sin[\alpha(x - x')]}{\pi(x - x')} \to \frac{\sin \frac{\pi}{\Delta}(x - x_k)}{\frac{\pi}{\Delta}(x - x_k)}. \tag{14}$$

In fact, not only the interpolating (or quasi-interpolating) nature guarantees the highest accuracy on the set of grid points, but also it provides the highest possible computational efficiency of a grid. This is because the Nyquist interval given by $[-\pi/\Delta, \pi/\Delta]$ is the largest possible sampling interval that is free of alias whenever an L^2 function $f(x)$ under study satisfies the Nyquist condition

$$\operatorname{supp} \hat{f}(k) \subset \left\{ -\frac{\pi}{\Delta}, \frac{\pi}{\Delta} \right\}. \tag{15}$$

This fact can be formally addressed by Shannon's sampling theorem

$$f(x) = \sum_{k=-\infty}^{\infty} f(x_k) \frac{\sin \frac{\pi}{\Delta}(x - x_k)}{\frac{\pi}{\Delta}(x - x_k)}. \tag{16}$$

The significance of Shannon's sampling theorem is that by a discrete, but infinite set of sampling data, $\{f(x_k)\}$, one can actually recover a bandlimited L^2 function on a real line. Such bandlimited L^2 functions are known as elements of the Paley–Wiener reproducing kernel Hilbert space. The discrete Shannon's kernels, $\left\{ \left(\sin \frac{\pi}{\Delta}(x - x_k)\right) / \left(\frac{\pi}{\Delta}(x - x_k)\right) \right\}_{k \in Z}$, are a complete set of sampling basis. Shannon's sampling theorem has great impact on information theory, signal and image processing because the Fourier transform of Shannon's wavelet kernel is an ideal low-pass filter for signals bandlimited to $[-\pi/\Delta, \pi/\Delta]$.

It is noted that the sequence of approximation can be improved by a regularizer (Wei, 1999a)

$$\lim_{\sigma \to \infty} R_\sigma(x) = 1. \tag{17}$$

The regularizer is designed to increase the regularity of convolution kernels. For the delta sequence, it follows from Eq. (8) that

$$\int \lim_{\alpha \to \alpha_0} T_\alpha(x) R_\sigma(x) \, \mathrm{d}x = R_\sigma(0) = 1, \tag{18}$$

where $R_\sigma(0) = 1$ is the special requirement for a *delta regularizer*. A typical delta regularizer used in this work and elsewhere (Wei, 1999a) is $\exp(-x^2/2\sigma^2)$. Therefore, Shannon's kernel is regularized as

$$\frac{\sin \frac{\pi}{\Delta}(x - x_k)}{\frac{\pi}{\Delta}(x - x_k)} \to \frac{\sin \frac{\pi}{\Delta}(x - x_k)}{\frac{\pi}{\Delta}(x - x_k)} \exp(-((x - x_k)^2/2\sigma^2)). \tag{19}$$

Since $\exp(-x^2/2\sigma^2)$ is a Schwartz class function, it makes the regularized kernel applicable to tempered distributions. Numerically, the regularized expression performs much better than Shannon's wavelet kernel for being used in a local approach for solving partial differential equations. Qian and Wei (submitted) have recently given a rigorous error estimation of the regularized formulae.

The uniform, Nyquist rate, interpolating discretization and the regularization are also adopted for the Dirichlet kernel:

$$\frac{\sin\left[\left(l + \frac{1}{2}\right)(x - x')\right]}{2\pi \sin\left[\frac{1}{2}(x - x')\right]} \to \frac{\sin\left(\frac{\pi}{\Delta}(x - x_k)\right)}{(2L + 1) \sin\left(\frac{\pi}{\Delta} \frac{x - x_k}{2L+1}\right)} \exp\left(-\frac{(x - x_k)^2}{2\sigma^2} \right). \tag{20}$$

In comparison to Shannon's kernel, the Dirichlet kernel has one more parameter L which can be optimized to achieve better results in computations. Usually, we set a sufficiently large L for various numerical applications. Obviously, the Dirichlet kernel converts to Shannon's kernel at the limit of $L \to \infty$. The uniform interpolating discretization and the regularization will also be used for the modified Dirichlet kernel

$$\frac{\sin\left[\left(l + \frac{1}{2}\right)(x - x')\right]}{2\pi \tan\left[\frac{1}{2}(x - x')\right]} \to \frac{\sin\left(\frac{\pi}{\Delta}(x - x_k)\right)}{(2L + 1) \tan\left(\frac{\pi}{\Delta} \frac{x - x_k}{2L+1}\right)} \exp\left(-\frac{(x - x_k)^2}{2\sigma^2} \right), \tag{21}$$

and for the de la Vallée Poussin kernel

$$\frac{1}{\pi\alpha}\frac{\cos[\alpha(x-x')]-\cos[2\alpha(x-x')]}{(x-x')^2}\to\frac{2}{3}\frac{\cos\frac{\pi}{\Delta}(x-x_k)-\cos\frac{2\pi}{\Delta}(x-x_k)}{\left[\frac{\pi}{\Delta}(x-x_k)\right]^2}\exp\left(-\frac{(x-x_k)^2}{2\sigma^2}\right), \tag{22}$$

where $\overline{\Delta}=\frac{3}{2}\Delta$. Since π/Δ is proportional to the highest frequency which can be reached in the Fourier representation, the Δ should be very small for a given problem involving highly oscillatory functions or very high frequency components.

We use a truncated singular kernel, which is symmetric or antisymmetric,

$$f^{(n)}(x)\approx\sum_{k=-M}^{M}\delta^{(n)}_{\alpha,\sigma}(x-x_k)f(x_k)\quad(n=0,1,2,\ldots), \tag{23}$$

where $2M+1$ is the computational bandwidth, or effective kernel support, which is usually smaller than the whole computational domain, $[a,b]$. Here $\delta^{(n)}_{\alpha,\sigma}(x-x_k)$ is a collective symbol for the nth derivative of any of the right-hand side of Eqs. (19)–(22). The differentiations in Eq. (23) can be easily carried out for a given $\delta_{\alpha,\sigma}(x-x_k)$. For example, if $\delta_{\frac{\pi}{\Delta},\sigma}(x-x_k)=\left(\sin\frac{\pi}{\Delta}(x-x_k)\right)/(\frac{\pi}{\Delta}(x-x_k))\exp(-(x-x_k)^2/(2\sigma^2))$, we have for $x\neq x_k$

$$\begin{aligned}\delta^{(1)}_{\frac{\pi}{\Delta},\sigma}(x-x_k)=&\frac{\cos\frac{\pi}{\Delta}(x-x_k)}{(x-x_k)}\exp\left(-\frac{(x-x_k)^2}{2\sigma^2}\right)-\frac{\sin\frac{\pi}{\Delta}(x-x_k)}{\frac{\pi}{\Delta}(x-x_k)^2}\exp\left(-\frac{(x-x_k)^2}{2\sigma^2}\right)\\&-\frac{\sin\frac{\pi}{\Delta}(x-x_k)}{\frac{\pi}{\Delta}\sigma^2}\exp\left(-\frac{(x-x_k)^2}{2\sigma^2}\right),\end{aligned} \tag{24}$$

$$\begin{aligned}\delta^{(2)}_{\frac{\pi}{\Delta},\sigma}(x-x_k)=&-\frac{\frac{\pi}{\Delta}\sin\frac{\pi}{\Delta}(x-x_k)}{(x-x_k)}\exp\left(-\frac{(x-x_k)^2}{2\sigma^2}\right)-2\frac{\cos\frac{\pi}{\Delta}(x-x_k)}{(x-x_k)^2}\exp\left(-\frac{(x-x_k)^2}{2\sigma^2}\right)\\&-2\frac{\cos\frac{\pi}{\Delta}(x-x_k)}{\sigma^2}\exp\left(-\frac{(x-x_k)^2}{2\sigma^2}\right)+2\frac{\sin\frac{\pi}{\Delta}(x-x_k)}{\frac{\pi}{\Delta}(x-x_k)^3}\exp\left(-\frac{(x-x_k)^2}{2\sigma^2}\right)\\&+\frac{\sin\frac{\pi}{\Delta}(x-x_k)}{\frac{\pi}{\Delta}(x-x_k)\sigma^2}\exp\left(-\frac{(x-x_k)^2}{2\sigma^2}\right)+\frac{\sin\frac{\pi}{\Delta}(x-x_k)}{\frac{\pi}{\Delta}\sigma^4}(x-x_k)\exp\left(-\frac{(x-x_k)^2}{2\sigma^2}\right),\end{aligned} \tag{25}$$

$$\begin{aligned}\delta^{(3)}_{\frac{\pi}{\Delta},\sigma}(x-x_k)=&-\frac{\frac{\pi^2}{\Delta^2}\cos\frac{\pi}{\Delta}(x-x_k)}{(x-x_k)}\exp\left(-\frac{(x-x_k)^2}{2\sigma^2}\right)+3\frac{\frac{\pi}{\Delta}\sin\frac{\pi}{\Delta}(x-x_k)}{(x-x_k)^2}\exp\left(-\frac{(x-x_k)^2}{2\sigma^2}\right)\\&+3\frac{\frac{\pi}{\Delta}\sin\frac{\pi}{\Delta}(x-x_k)}{\sigma^2}\exp\left(-\frac{(x-x_k)^2}{2\sigma^2}\right)+6\frac{\cos\frac{\pi}{\Delta}(x-x_k)}{(x-x_k)^3}\exp\left(-\frac{(x-x_k)^2}{2\sigma^2}\right)\\&+3\frac{\cos\frac{\pi}{\Delta}(x-x_k)}{(x-x_k)\sigma^2}\exp\left(-\frac{(x-x_k)^2}{2\sigma^2}\right)+3\frac{(x-x_k)\cos\frac{\pi}{\Delta}(x-x_k)}{\sigma^4}\exp\left(-\frac{(x-x_k)^2}{2\sigma^2}\right)\\&-6\frac{\sin\frac{\pi}{\Delta}(x-x_k)}{\frac{\pi}{\Delta}(x-x_k)^4}\exp\left(-\frac{(x-x_k)^2}{2\sigma^2}\right)-3\frac{\sin\frac{\pi}{\Delta}(x-x_k)}{\frac{\pi}{\Delta}(x-x_k)^2\sigma^2}\exp\left(-\frac{(x-x_k)^2}{2\sigma^2}\right)\\&-\frac{(x-x_k)^2\sin\frac{\pi}{\Delta}(x-x_k)}{\frac{\pi}{\Delta}\sigma^6}\exp\left(-\frac{(x-x_k)^2}{2\sigma^2}\right)\end{aligned} \tag{26}$$

and

$$\delta^{(4)}_{\frac{\pi}{\Delta},\sigma}(x-x_k) = 4\frac{\frac{\pi^2}{\Delta^2}\cos\frac{\pi}{\Delta}(x-x_k)}{(x-x_k)^2}\exp\left(-\frac{(x-x_k)^2}{2\sigma^2}\right) + \frac{\frac{\pi^3}{\Delta^3}\sin\frac{\pi}{\Delta}(x-x_k)}{(x-x_k)}\exp\left(-\frac{(x-x_k)^2}{2\sigma^2}\right)$$
$$+ 4\frac{\frac{\pi^2}{\Delta^2}\cos\frac{\pi}{\Delta}(x-x_k)}{\sigma^2}\exp\left(-\frac{(x-x_k)^2}{2\sigma^2}\right) - 12\frac{\frac{\pi}{\Delta}\sin\frac{\pi}{\Delta}(x-x_k)}{(x-x_k)^3}\exp\left(-\frac{(x-x_k)^2}{2\sigma^2}\right)$$
$$- 6\frac{\frac{\pi}{\Delta}\sin\frac{\pi}{\Delta}(x-x_k)}{(x-x_k)\sigma^2}\exp\left(-\frac{(x-x_k)^2}{2\sigma^2}\right) - 6\frac{\frac{\pi}{\Delta}(x-x_k)\sin\frac{\pi}{\Delta}(x-x_k)}{\sigma^4}$$
$$\times\exp\left(-\frac{(x-x_k)^2}{2\sigma^2}\right) - 24\frac{\cos\frac{\pi}{\Delta}(x-x_k)}{(x-x_k)^4}\exp\left(-\frac{(x-x_k)^2}{2\sigma^2}\right) - 12\frac{\cos\frac{\pi}{\Delta}(x-x_k)}{(x-x_k)^2\sigma^2}$$
$$\times\exp\left(-\frac{(x-x_k)^2}{2\sigma^2}\right) - 4\frac{(x-x_k)^2\cos\frac{\pi}{\Delta}(x-x_k)}{\sigma^6}\exp\left(-\frac{(x-x_k)^2}{2\sigma^2}\right) + 24\frac{\sin\frac{\pi}{\Delta}(x-x_k)}{\frac{\pi}{\Delta}(x-x_k)^5}$$
$$\times\exp\left(-\frac{(x-x_k)^2}{2\sigma^2}\right) + 12\frac{\sin\frac{\pi}{\Delta}(x-x_k)}{\frac{\pi}{\Delta}(x-x_k)^3\sigma^2}\exp\left(-\frac{(x-x_k)^2}{2\sigma^2}\right) + 3\frac{\sin\frac{\pi}{\Delta}(x-x_k)}{\frac{\pi}{\Delta}(x-x_k)\sigma^4}$$
$$\times\exp\left(-\frac{(x-x_k)^2}{2\sigma^2}\right) - 2\frac{(x-x_k)\sin\frac{\pi}{\Delta}(x-x_k)}{\frac{\pi}{\Delta}\sigma^6}\exp\left(-\frac{(x-x_k)^2}{2\sigma^2}\right)$$
$$+ \frac{(x-x_k)^3\sin\frac{\pi}{\Delta}(x-x_k)}{\frac{\pi}{\Delta}\sigma^8}\exp\left(-\frac{(x-x_k)^2}{2\sigma^2}\right). \tag{27}$$

At $x = x_k$, it is convenient to evaluate these derivatives separately

$$\delta^{(1)}_{\frac{\pi}{\Delta},\sigma}(0) = 0, \tag{28}$$

$$\delta^{(2)}_{\frac{\pi}{\Delta},\sigma}(0) = -\frac{1}{3}\frac{3+\frac{\pi}{\Delta}\sigma^2}{\sigma^2} = 20, \tag{29}$$

$$\delta^{(3)}_{\frac{\pi}{\Delta},\sigma}(0) = 0 \tag{30}$$

and

$$\delta^{(4)}_{\frac{\pi}{\Delta},\sigma}(0) = \frac{1}{5}\frac{15+10\frac{\pi^2}{\Delta^2}\sigma^2+\frac{\pi^4}{\Delta^4}\sigma^4}{\sigma^4}. \tag{31}$$

Qian and Wei (submitted) have recently provided a mathematical estimation for the choice of M, σ and Δ. For example, if the L_2 error for approximating an L^2 function f is set to $10^{-\eta}$ ($\eta > 0$), the following relations are to be satisfied

$$r(\pi - B\Delta) > \sqrt{4.61\eta} \quad \text{and} \quad \frac{M}{r} > \sqrt{4.61\eta}, \tag{32}$$

where $r = \sigma/\Delta$ and B is the frequency bound for the function of interest, f. The first inequality states that for a given grid size Δ, a large r is required for approximating high frequency component of an L^2 function. The second inequality indicates that if one chooses the ratio $r = 3$, then the half bandwidth $M \sim 30$ can be used to ensure the highest accuracy in a double precision computation ($\eta = 15$). This theoretical estimation is in very good agreement with a previous numerical test (Wei, 2000b).

2.3. Vibration analysis of plates by using the discrete singular convolution

Consider a general operator $\mathscr{O}$ having a differential part $\mathscr{D}$ and a function part F

$$\mathscr{O} = \mathscr{D} + F. \tag{33}$$

In the DSC approach, it is convenient to choose a grid representation for the coordinate so that the function part F of the operator is diagonal. Hence, its discretization is simply given by a direct interpolation on the grid

$$F(x) \to F(x_k)\delta_{m,k}. \tag{34}$$

The differential part of the operator on the coordinate grid is then represented by functional derivatives

$$\mathscr{D} = \sum_n d_n(x)\frac{\mathrm{d}^n}{\mathrm{d}x^n} \to \sum_n d_n(x_m)\delta^{(n)}_{\alpha,\sigma}(x_m - x_k), \tag{35}$$

where $d_n(x)$ is a coefficient and $\delta^{(n)}_{\alpha,\sigma}(x_m - x_k)$ is *analytically* given by

$$\delta^{(n)}_{\alpha,\sigma}(x_m - x_k) = \left[\left(\frac{\mathrm{d}}{\mathrm{d}x}\right)^n \delta_{\alpha,\sigma}(x - x_k)\right]_{x=x_m}. \tag{36}$$

Here $\delta_{\alpha,\sigma}(x - x_k)$ is a collective symbol for the right-hand sides of Eqs. (19)–(22).

Note that the differentiation matrix in Eq. (35) is in general banded. This gives rise to great advantage in large scale computations. Moveover, the DSC kernels are translationally invariant in the computational domain. Therefore, it is very simple to implement. Extension to higher dimensions can be realized by tensorial products. We refer expression (36) and its higher dimensional generalizations as DSC matrices.

Although many excellent DSC kernels are constructed for numerical computations, we focus on the following discretized form of the regularized Shannon's wavelet kernel

$$\delta_{\frac{\pi}{\Delta},\sigma}(x - x_j) = \frac{\sin\frac{\pi}{\Delta}(x - x_j)}{\frac{\pi}{\Delta}(x - x_j)}\exp(-(x - x_j)^2/(2\sigma^2)) \tag{37}$$

to illustrate the algorithm and its application to high frequency vibration analysis. Nevertheless, various other DSC kernels can be similarly employed (Wei, 1999a). The performance of a few DSC kernels for fluid dynamic computations and structural analysis was compared in Wei (2001a).

For generality and simplicity, the following dimensionless parameters are introduced for a rectangular plate

$$X = \frac{x}{a},\quad Y = \frac{y}{b},\quad W = \frac{w}{a};\quad \lambda = \frac{a}{b};\quad \Omega = \omega a^2\sqrt{\frac{\rho h}{D}}. \tag{38}$$

In terms of Eq. (38), the governing differential equation for vibration of plate (i.e., Eq. (2)) can be expressed in the dimensionless form as

$$\frac{\partial^4 W}{\partial X^4} + 2\lambda^2\frac{\partial^4 W}{\partial X^2\,\partial Y^2} + \lambda^4\frac{\partial^4 W}{\partial Y^4} = \Omega^2 W. \tag{39}$$

Consider a uniform grid having

$$0 = X_0 < X_1 < \cdots < X_{N_X} = 1$$

and

$$0 = Y_0 < Y_1 < \cdots < Y_{N_Y} = 1.$$

To formulate the eigenvalue problem, we introduce a column vector $\mathbf{W}$ as

$$\mathbf{W} = (W_{0,0}, \ldots, W_{0,N_Y}, W_{1,0}, \ldots, W_{N_X,N_Y})^{\mathrm{T}} \tag{40}$$

with $(N_X+1)(N_Y+1)$ entries $W_{i,j} = W(X_i, Y_j)$ $(i = 0, 1, \ldots, N_X;\ j = 0, 1, \ldots, N_Y)$.

Let us define the $(N_q+1) \times (N_q+1)$ differentiation matrices $\mathbf{D}_q^n$ $(q = X, Y;\ n = 1, 2, \ldots)$, with their elements given by

$$\left[\mathbf{D}_q^n\right]_{i,j} = \delta^{(n)}_{\frac{\pi}{\Delta},\sigma}(q_i - q_j) \quad (i, j = 0, \ldots, N_q), \tag{41}$$

where $\delta_{\sigma,\Delta}(q_i - q_j)$ is obtained from the regularized Shannon's wavelet kernel (37). The differentiation in Eq. (41) can be *analytically* carried out

$$\delta^{(n)}_{\frac{\pi}{\Delta},\sigma}(q_i - q_j) = \left[\left(\frac{\mathrm{d}}{\mathrm{d}q}\right)^n \delta_{\frac{\pi}{\Delta},\sigma}(q - q_j)\right]_{q=q_i} = C_m^n, \tag{42}$$

where, for a uniform grid spacing, $m = (q_i - q_j)/\Delta$. Here the matrix is banded to $i - j = m = -M, \ldots, 0, \ldots, M$. Therefore, in the matrix notation, the governing eigenvalue equation (39) is given by

$$\left(\mathbf{D}_X^4 \otimes \mathbf{I}_Y + 2\lambda^2 \mathbf{D}_X^2 \otimes \mathbf{D}_Y^2 + \lambda^4 \mathbf{I}_X \otimes \mathbf{D}_Y^4\right)\mathbf{W} = \Omega^2 \mathbf{W}, \tag{43}$$

where $\mathbf{I}_q$ is the $(N_q+1)^2$ unit matrix and $\otimes$ denotes the tensorial product. Eigenvalues can be evaluated from Eq. (43) by using a standard solver. However, appropriate boundary conditions need to be implemented before the eigenvalues can be obtained. This is described below.

We first note that boundary condition $W = 0$ is easily specified at the edge. To implement other boundary conditions, we assume, for a function f, the following relation between the inner nodes and the outer nodes on the left boundary

$$f(X_{-m}) - f(X_0) = \left(\sum_{j=0}^{J} a_m^j X_m^j\right)[f(X_m) - f(X_0)], \tag{44}$$

where coefficients a_m^j $(m = 1, \ldots, M, j = 0, 1, \ldots, J)$ are to be determined by the boundary conditions. For the two types of boundary conditions described earlier, we only need to consider the zeroth order term in the power of X^j. Therefore we set $a_m^0 \equiv a_m$ and, after rearrangement, obtain

$$f(X_{-m}) = a_m f(X_m) + (1 - a_m) f(X_0), \quad m = 1, 2, \ldots, M. \tag{45}$$

According to Eq. (42), the first and the second derivatives of f on the boundary are approximated by

$$\begin{aligned} f'(X_0) &= \sum_{m=-M}^{M} C_m^1 f(X_m) \\ &= \left[C_0^1 - \sum_{m=1}^{M}(1 - a_m) C_m^1\right] f(X_0) + \sum_{m=1}^{M}(1 - a_m) C_m^1 f(X_m) \end{aligned} \tag{46}$$

and

$$f''(X_0) = \sum_{m=-M}^{M} C_m^2 f(X_m) = \left[C_0^2 + \sum_{m=1}^{M}(1 - a_m) C_m^2\right] f(X_0) + \sum_{m=1}^{M}(1 + a_m) C_m^2 f(X_m), \tag{47}$$

respectively.

For simply supported edges, the boundary conditions may be reduced to

$$f(X_0) = 0, \quad f''(X_0) = 0. \tag{48}$$

These are satisfied by choosing $a_m = -1, m = 1, 2, \ldots, M$. This is the so-called *antisymmetric extension*.

For clamped edges, the boundary conditions require

$$f(X_0) = 0, \quad f'(X_0) = 0. \tag{49}$$

These are satisfied by $a_m = 1, m = 1, 2, \ldots, M$. This is the *symmetric extension*.

2.4. The Levy method

In the Levy method, a rectangular plate is assumed to be simply supported on the two opposite edges parallel to the x-axis. The other two edges may take any combination of edge conditions. The displacement function for the plate may be expressed as

$$w(x, y) = \sin\left(\frac{m\pi}{b}y\right)Z(x), \tag{50}$$

where m is the number of half waves of the vibration mode in the y-direction. Eq. (50) satisfies the boundary conditions for the two simply supported edges at $y = 0$ and b.

In view of Eqs. (50) and (2), a homogeneous differential equation system for the plate can be derived as follows

$$\boldsymbol{\Psi}^{(1)} - \mathbf{H}\boldsymbol{\Psi} = \mathbf{0}, \tag{51}$$

where

$$\boldsymbol{\Psi} = \begin{Bmatrix} Z \\ Z^{(1)} \\ Z^{(2)} \\ Z^{(3)} \end{Bmatrix} \tag{52}$$

and the superscript denotes differentiation with respect to x. Here, $\mathbf{H}$ is a 4×4 matrix and its non-zero elements are given by

$$\begin{aligned} &H_{12} = H_{23} = H_{34} = 1, \\ &H_{41} = \frac{\rho b\omega^2}{D} - \left(\frac{m\pi}{b}\right)^4, \\ &H_{43} = 2\left(\frac{m\pi}{b}\right)^2. \end{aligned} \tag{53}$$

The procedure for solving Eq. (51) has been detailed by Xiang et al. (1996) and the solution of Eq. (51) can be expressed as

$$\boldsymbol{\Psi} = \exp(\mathbf{H}x)\mathbf{c}, \tag{54}$$

where $\exp(\mathbf{H}x)$ is a general solution matrix of Eq. (51); $\mathbf{c}$ is a four-component constant column vectors, which can be determined by the boundary conditions of the plate along the two edges parallel to the y-axis.

In view of Eq. (54), a homogeneous system of equations can be derived after considering the boundary conditions of the plate (Xiang et al., 1996):

$$\mathbf{K}\mathbf{c} = \mathbf{0}, \tag{55}$$

where $\mathbf{K}$ is a 4×4 matrix. The vibration frequency ω is evaluated by setting the determinant of $\mathbf{K}$ to zero.

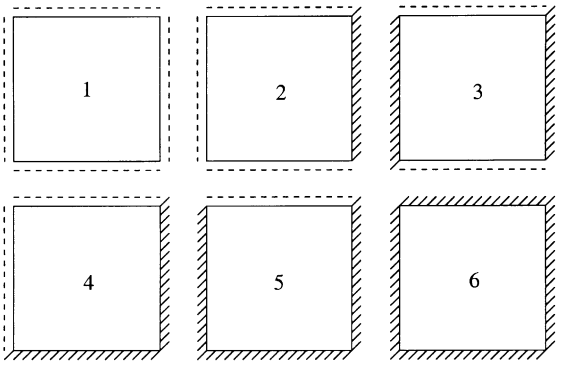

Fig. 1. Cases 1–6 of square plates with different edge supports.

3. Results and discussion

The application of the DSC method to high frequency vibration analysis is demonstrated in this section through extensive numerical studies on vibration of square plates. Fig. 1 depicts six distinct boundary conditions which are obtained by a combination of simply supported and clamped edges. The Poisson ratio is taken as 0.3 when needed. Frequency parameters are computed for all the six cases by using the DSC algorithm. Case 1 is analytically solvable and its non-trivial frequency parameters are explicitly reported as

$$\frac{\Omega_{n_x,n_y}}{\pi^2} = n_x^2 + n_y^2 \quad (n_x, n_y = 1, 2, \ldots), \tag{56}$$

where n_x and n_y are the number of half waves of the solution in the x- and y-directions, respectively. For other cases, no analytical solution is *explicitly* available. However, for Cases 2 and 3, the Levy approach is readily available to give an exact solution. As it is well-known that such an exact solution can be arbitrarily accurate. To test the reliability of the present Levy code, the complete set of the first 7755 modes for Case 1 have been computed against the analytical solution. Our Levy results are indeed reliable and arbitrarily accurate. As such, the Levy method is employed to provide exact solutions for Cases 2 and 3. Such solutions are utilized for a cross-validation of the DSC results.

3.1. Convergence and comparison studies

3.1.1. Convergence and error analysis of Case 1

To verify the validity and accuracy of the proposed DSC approach, convergence and comparison studies are first carried out for a simply supported square plate (Case 1). DSC calculations are performed on a number of grids, ranging from 11^2 to 101^2 points. The convergence study of the DSC results are summarized in Table 1. Both the DSC results and analytical ones are ordered according to their magnitudes. When the DSC grid is 31^2, the first 100 modes are firmly converged. Such a result is consistent with a previous study (Wei, 1999c) where an 11 significant-figure accuracy was achieved by using both the regularized Shannon kernel and the regularized Dirichlet kernel with a grid of 33^2 points. With a grid of 41^2, the first 500 modes have converged to four significant figures. An accuracy of five significant figures is reached for the first 1000 modes at the grid of 61^2 points and similar accuracy is obtained for the first 2000 modes at the grid of 91^2 points. It is noted that p-version FEM of Bardell (1991) can only be used for computing the first 390 modes and the best HFEM (Langley and Bardell, 1998) predicts only up to about

Table 1
Convergence and comparison of the frequency parameters for a SSSS square plate

Mode number	Mesh size										Analytical solution
	11^2	21^2	31^2	41^2	51^2	61^2	71^2	81^2	91^2	101^2	
1	1.9810	2.0000	2.0000	2.0000	2.0000	2.0000	2.0000	2.0000	2.0000	2.0000	2
10	17.1561	17.0000	17.0000	17.0000	17.0000	17.0000	17.0000	17.0000	17.0000	17.0000	17
50	80.5695	73.0089	73.0000	73.0000	73.0000	73.0000	73.0000	73.0000	73.0000	73.0000	73
100	–	145.0328	145.0000	145.0000	145.0000	145.0000	145.0000	145.0000	145.0000	145.0000	145
300	–	444.4968	408.9885	405.0003	405.0000	405.0000	405.0000	405.0000	405.0000	405.0000	405
500	–	–	699.8320	673.0794	673.0008	673.0000	673.0000	673.0000	673.0000	673.0000	673
700	–	–	1002.1186	933.0693	928.0721	928.0016	928.0001	928.0000	928.0000	928.0000	928
1000	–	–	–	1379.4256	1322.6174	1314.0682	1314.0027	1314.0002	1314.0000	1314.0000	1314
1500	–	–	–	2812.8155	2050.0637	1974.4049	1962.9583	1962.0073	1962.0006	1962.0001	1962
2000	–	–	–	–	2777.4345	2685.9807	2623.5894	2609.5380	2609.0480	2609.0053	2609
2500	–	–	–	–	–	3434.3055	3309.7592	3272.2801	3256.8198	3253.4827	3253
3000	–	–	–	–	–	4238.8166	4072.9801	3949.2765	3899.3705	3893.6414	3893
3500	–	–	–	–	–	–	4789.3601	4663.7991	4573.5879	4545.3831	4538
4000	–	–	–	–	–	–	5542.1399	5422.1877	5256.1279	5205.5699	5188
4500	–	–	–	–	–	–	7168.4286	6153.4761	6003.9363	5873.3290	5825
5000	–	–	–	–	–	–	–	6788.8985	6756.1822	6574.9959	6466

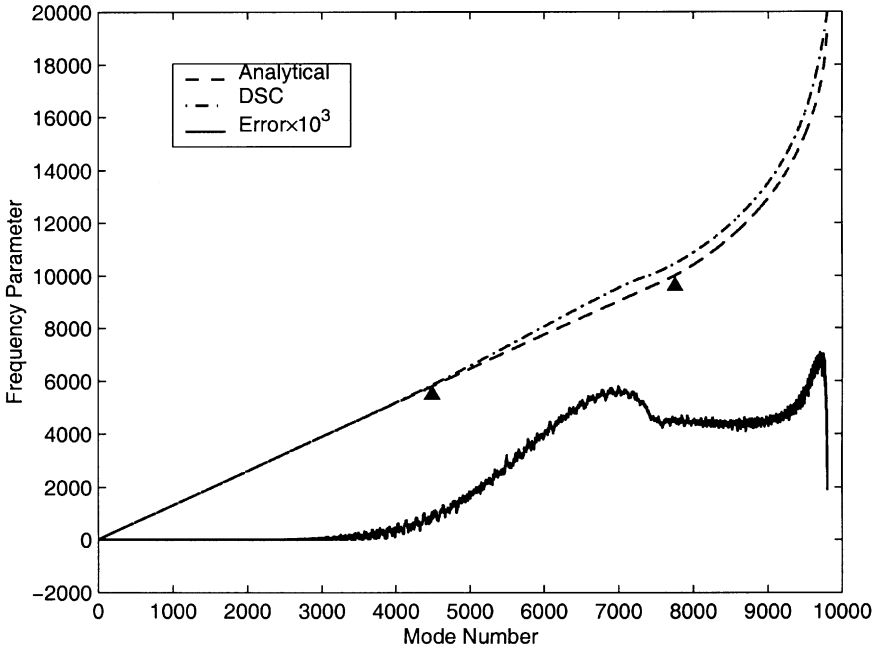

Fig. 2. Comparison of DSC and analytical frequency parameters and their relative errors versus the mode numbers for an SSSS square plate (Case 1).

the 850th mode for this case, due to the numerical instability of their matrices. Obviously, the DSC results are remarkable and the best ever attained for this problem.

It is interesting to explore the limit of the DSC algorithm for the prediction of high frequency vibration. To study such a problem, we plotted in Fig. 2 the DSC results against a subset of the analytical solution, generated by setting $1 \leqslant n_x \leqslant 99$, $1 \leqslant n_y \leqslant 99$. Such a subset is chosen because the DSC grid of 101 points in each dimension supports at most 99 half waves due to the simply supported or clamped edges. For the analytical results, the frequency parameter scales essentially linear with the mode number when the frequency parameter is smaller than 10,001. This value corresponds to $n_x = 100$, $n_y = 1$ and is the first missing value due to the present restriction to the subset. The corresponding mode number is 7755 as marked in Fig. 2. The frequency parameter increases dramatically as the mode number exceeds the critic point. This is because more and more modes are missing when using Eq. (56) associated with the limit $n_x \leqslant 99$, $n_y \leqslant 99$. The DSC results compare extremely well with the analytical results up to the frequency parameter of 4490, which corresponds to $n_x = 67$, $n_y = 1$. Theoretically, no numerical method can beat the Nyquist frequency limit $(\pi/\Delta) = \pi n_x$ without incurring aliasing errors. Such a frequency limit corresponds to about two internal grid points per wavelength, which support two local extrema. The DSC algorithm is accurate up to five significant figures if there are four internal grid points per wavelength, i.e., all modes given by $n_x \leqslant 50$, $n_y \leqslant 50$ in the present computation using a grid of 101^2 points. If the grid is reduced to three points per wavelength, i.e., all modes given by $n_x < 67$, $n_y < 67$, the DSC results are still accurate to three significant figures, which corresponds to less than 1% of relative errors. Such a result is very reliable for the purpose of most engineering designs. The mode, corresponding to $n_x = 67$, $n_y = 1$, is mode 3452 and is also marked in Fig. 2. Although after mode 3452 the DSC errors are getting larger, as seen from Fig. 2 due to considerable aliasing errors, the largest DSC error is less than 6% before the critical mode 7755. After the critical mode 7755, the restricted analytical frequency parameters start to miss modes. Even in this after critical region,

the relative DSC errors are still less than 7%. Certainly, neither the restricted analytical results, nor the DSC results, are reliable after the critical mode.

Fig. 3(a) presents a contour plot of the modal shape for the 5002nd mode. This modal shape is plotted on a data size of 401^2, which is generated from the original numerical data by an interpolation using the same

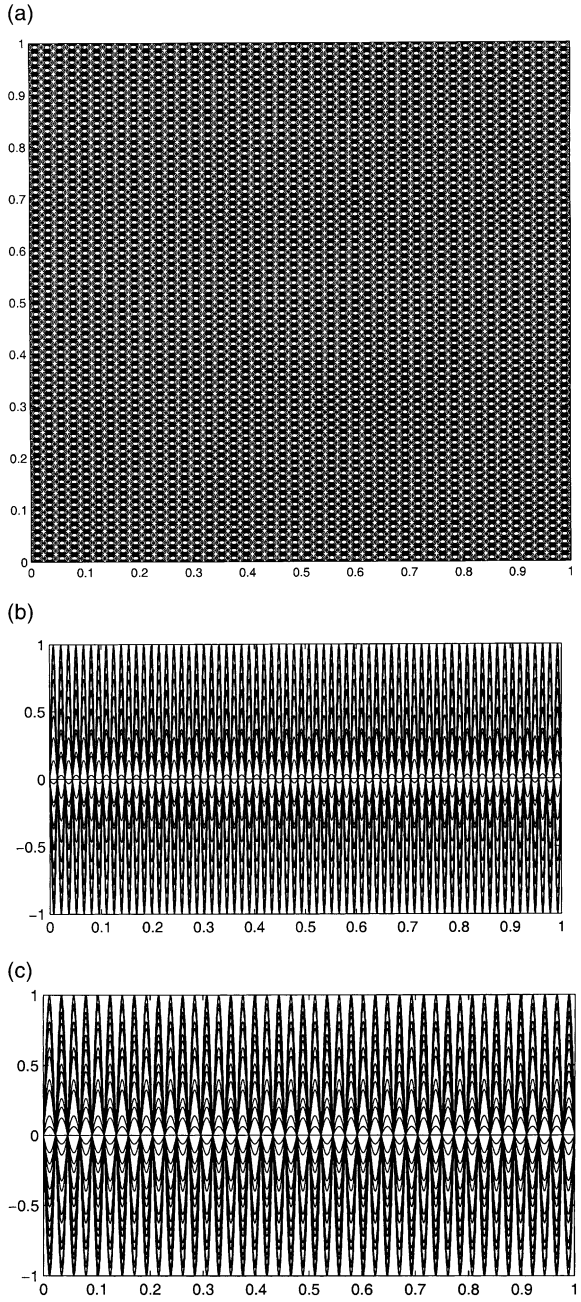

Fig. 3. The 5002nd mode of Case 1: (a) contour plot; (b) side view along y-axis; (c) side view along x-axis.

DSC algorithm as the interpolating kernel. The numerical error of frequency parameter for the plotted mode is 1.7%. The side view of this mode is given in Fig. 3(b) and (c). It is seen that the modal shape is extremely regular. There is no visible numerical errors as those in Fig. 10 for the 850th mode given by Beslin and Nicolas (1997). In fact, all the first 4518 DSC modes have less than 1% numerical errors and their modal shapes do not shown any visible irregularity.

3.1.2. Convergence studies of Cases 3 and 5

Having built up our confidence with the DSC approach for the four-edge simply supported plates, it is necessary to further test the reliability level of the DSC high frequency prediction for other support conditions. To this end, we choose Cases 3 and 5 as our next test examples. Case 3 admits the Levy solution, and thus has an exact solution, which provides another objective test for the proposed DSC approach. It is also important to examine the behavior of the DSC algorithm for a class of real vibration problems that are not analytical solvable. Therefore, Case 5 is selected for the convergence studies.

The convergence studies for Cases 3 and 5 are pursued with a number of DSC grids, ranging from 11^2 to 101^2 points. We have checked the speed of convergence for the first few thousand modes. These results are listed in Tables 2 and 3 for Cases 3 and 5, respectively. Obviously, these DSC results converge to the Levy solution for Case 3. The relative errors of DSC results against the Levy solution is plotted in Fig. 4. As seen from Table 2, the first 100 modes have converged at the grid of 31^2 points. The degree of convergence in these modes is not as firm as that in Case 1 for the same level of computation. The first 500 modes converge to less than 0.1% relative errors at the grid of 51^2 points. Like in Case 1, it takes a grid as large as 61^2 points to obtain a converged results for the first 1000 modes with relative errors less than 0.3%. Remarkably, the relative errors of the first 2000 modes are less than 0.02% at the DSC grid of 91^2 points. At the final grid of 101^2 points, the relative errors of first 2500 and 3000 modes are less than 0.2% and 0.3%, respectively. In fact, the relative errors for the first 4000 and 5000 modes are less than 0.7% and 2%, respectively on this grid. To the left of mode 3500, the DSC results for Case 1 are more accurate than those for Case 3. However, the error distribution in Cases 1 and 3 are extremely similar to each other to the right of mode 3500. For example, the maximum relative error is less than 6% for all modes to the left of mode 7755. Such a result indicates that the solution of the DSC algorithm is very reliable for the first 40% modes computed and is quite reliable for the modes filling between the first 40–50% (within 2% errors). This can be seen by examining the modal shape of Case 3, as depicted in Fig. 5. Unlike the mode in Fig. 3, this mode has many half waves in one direction, but has fewer half waves in the other direction. However, the mode is extremely regular and no visible error can be seen. The DSC results become less reliable, but are still useful for the modes filling between the first 50–75%. Although the last 25% modes are unreliable for being used quantitatively. However, the tendency of the DSC results for that section is still reasonable.

The convergence pattern of Case 5 is almost identical to that of Case 3. This can be easily confirmed by a comparison of the speed of convergence in Tables 2 and 3. For example, for mode 2500 of Case 3, the relative errors at grids of 61^2, 71^2, 81^2, 91^2, with respect to the result obtained by the grid of 101^2 are: 5.6772%, 2.3767%, 0.2928%, and 0.0487%. The corresponding errors of Case 5 are 5.6638%, 2.2233%, 0.5152%, and 0.0304%. Such a great similarity between the DSC results of Cases 3 and 5 supports our general discussion about the reliability of the DSC algorithm given in the last paragraph.

3.2. Case studies

The convergence and comparison studies in previous subsection have confirmed the validity and accuracy of the DSC algorithm for the high frequency analysis of square plates with simply supported edges and clamped edges and their combinations. The purpose of the present subsection is to report more detailed frequency parameters which are unavailable in any existing literature, due to the lack of stable and reliable

Table 2
Convergence and comparison of the frequency parameters for a CSCS square plate

Mode number	Mesh size										Levy's solution
	11^2	21^2	31^2	41^2	51^2	61^2	71^2	81^2	91^2	101^2	
1	2.9405	2.9338	2.9334	2.9334	2.9334	2.9333	2.9333	2.9333	2.9333	2.9333	2.9333
10	20.4944	20.2610	20.2494	20.2467	20.2459	20.2455	20.2454	20.2453	20.2452	20.2451	20.2450
50	88.7431	77.0207	76.9206	76.8957	76.8875	76.8838	76.8819	76.8809	76.8802	76.8798	76.8786
100	–	149.9107	148.0682	148.0240	148.0086	148.0014	147.9977	147.9956	147.9942	147.9934	147.9911
300	–	457.9526	421.7334	416.0358	415.8761	415.7992	415.7578	415.7337	415.7187	415.7090	415.6817
500	–	–	725.3513	681.4443	680.1673	680.0382	679.7974	679.6641	679.6442	679.6311	679.5931
700	–	–	1018.5092	957.3923	944.5066	944.2306	944.1605	944.1198	944.0937	944.0762	944.0245
1000	–	–	–	1412.4055	1346.9832	1337.0680	1335.0782	1334.6971	1334.4611	1334.3067	1333.8679
1500	–	–	–	2848.4010	2080.5595	2005.9067	1991.3757	1987.4015	1987.1079	1986.9106	1986.3091
2000	–	–	–	–	2814.2936	2728.1499	2650.4802	2641.1468	2638.0373	2637.7231	2637.6402
2500	–	–	–	–	–	3472.1971	3363.7538	3295.2845	3287.2640	3285.6637	3283.0935
3000	–	–	–	–	–	4275.8963	4110.6715	3985.4031	3941.6742	3930.6642	3926.1786
3500	–	–	–	–	–	–	4822.2977	4717.7817	4610.3545	4585.8606	4572.0996
4000	–	–	–	–	–	–	5574.0580	5477.6402	5311.8317	5245.0007	5220.45308
4500	–	–	–	–	–	–	7220.1386	6198.9577	6048.5916	5925.5958	5867.86558
5000	–	–	–	–	–	–	–	6828.4774	6814.3333	6633.3643	6504.21895

Table 3
Convergence of frequency parameters for a CCCS square plate

Mode number	Mesh size										Analytical solution
	11^2	21^2	31^2	41^2	51^2	61^2	71^2	81^2	91^2	101^2	
1	3.2388	3.2252	3.2248	3.2247	3.2247	3.2247	3.2247	3.2247	3.2247	3.2247	NA
10	21.5405	21.2317	21.2152	21.2114	21.2102	21.2097	21.2094	21.2093	21.2092	21.2091	NA
50	90.8605	79.8541	79.6678	79.6234	79.6089	79.6024	79.5991	79.5972	79.5961	79.5953	NA
100	–	154.3896	153.1182	152.9901	152.9487	152.9300	152.9203	152.9148	152.9115	152.9093	NA
300	–	460.4169	427.0778	422.1673	421.6941	421.5009	421.4042	421.3502	421.3177	421.2969	NA
500	–	–	730.8059	689.9917	689.0260	688.6682	688.4808	688.3726	688.3056	688.2621	NA
700	–	–	1030.4138	965.2237	953.6379	952.2376	951.7077	951.4211	951.2489	951.1388	NA
1000	–	–	–	1421.4820	1357.4599	1346.1118	1345.2574	1344.9086	1344.7090	1344.5529	NA
1500	–	–	–	2862.3984	2096.4358	2019.4815	2002.7030	1999.0437	1997.9926	1997.4696	NA
2000	–	–	–	–	2823.3398	2747.1305	2670.5988	2652.5601	2649.1251	2648.3326	NA
2500	–	–	–	–	–	3489.9133	3376.2781	3319.8629	3303.8514	3302.8475	NA
3000	–	–	–	–	–	4296.6772	4139.7335	4011.2886	3956.8308	3946.0218	NA
3500	–	–	–	–	–	–	4840.4963	4740.6079	4634.5845	4599.1441	NA
4000	–	–	–	–	–	–	5598.1785	5501.8295	5345.5062	5268.6322	NA
4500	–	–	–	–	–	–	7247.8570	6218.7360	6077.9785	5949.7340	NA
5000	–	–	–	–	–	–	–	6844.1909	6846.4239	6661.4364	NA

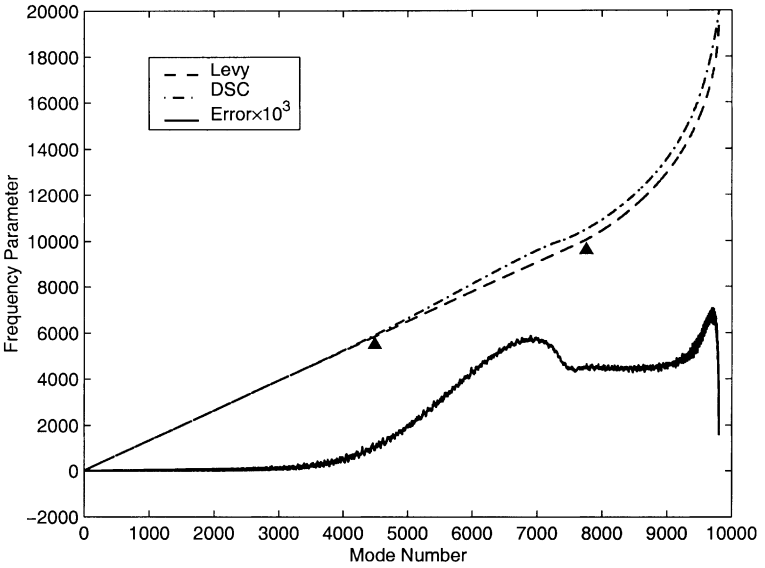

Fig. 4. Comparison of DSC and analytical frequency parameters and their relative errors versus the mode numbers for a CSCS square plate (Case 3).

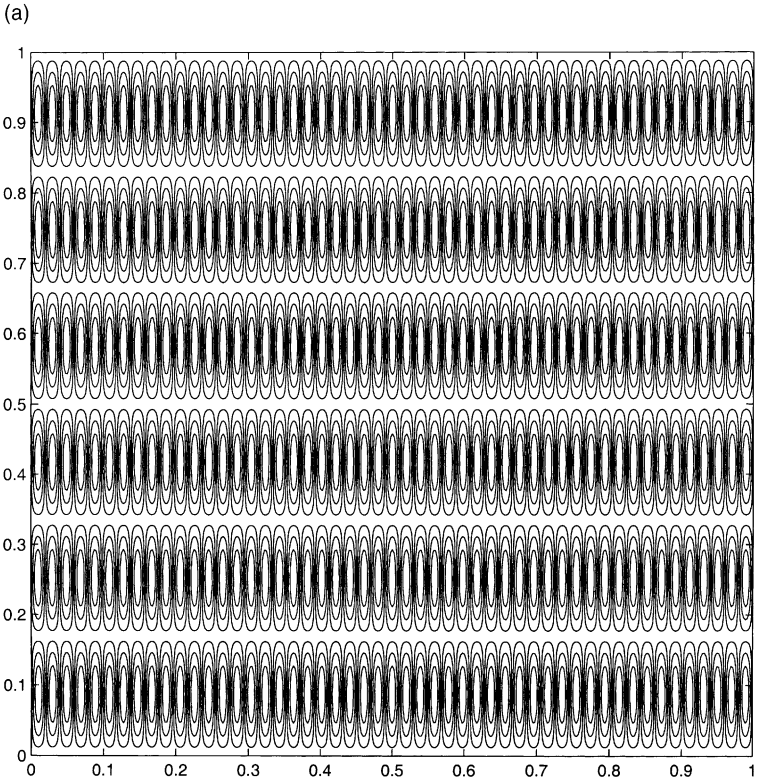

Fig. 5. The 2000th mode of Case 3: (a) contour plot; (b) side view along y-axis; (c) side view along x-axis.

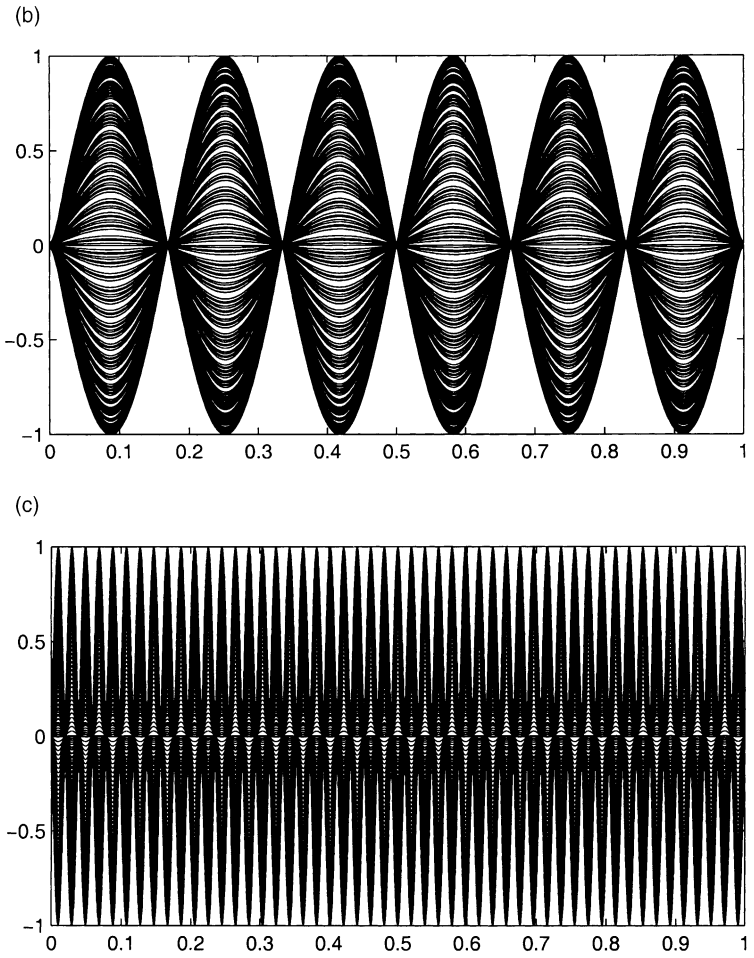

Fig. 5 (*continued*)

numerical methods. The present study focuses on the last five cases in Fig. 1, since the analytical solution is available for Case 1.

The Levy solution, the DSC solution, and the relative error of Case 2 are plotted in Fig. 6. Obviously, the plot confirms the consistence of the DSC algorithm for all the three analytically solvable cases as both the magnitude and trend of the error are essentially identical to those of the DSC results for Case 3. Since the first 5000 DSC modes computed by using the grid of 101^2 points have less than 2% relative errors, it is reasonable to recommend that the DSC algorithm prediction associated with proper plate theories can be used to analyze high frequency vibration of plates and the results can be used in most engineering designs. What is encouraged is the fact that, in case a better precision is required, it is very robust to fulfill such a requirement by increasing the number of the DSC grid points.

In fact, the Levy solutions for high frequency vibration of Cases 2 and 3 have not been reported previously, and thus they are valuable for objectively testing new potential numerical methods for high frequency analysis. The DSC results for Cases 4–6 are of benchmark quality for their first 5000 modes. It is believed that these DSC results are valuable for numerical test of other potential methods. For these

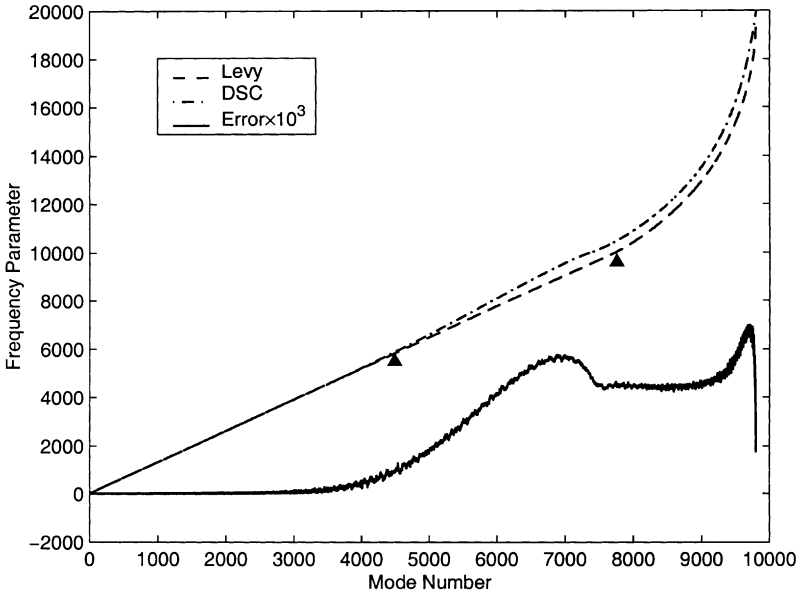

Fig. 6. Comparison of DSC and analytical frequency parameters and their relative errors versus the mode numbers for an SSCS square plate (Case 2).

reasons, we have summarized the DSC results of Cases 2–5 and the Levy solutions of Cases 2 and 3, up to mode 5000, in Table 4. The detailed half wave information for the Levy solution is also given in Table 4.

4. Conclusion

High frequency vibration prediction is a challenging task in structural analysis and optimization. The lack of stable and reliable numerical methods for the prediction has been a long standing problem due to numerical round-off in conventional numerical approaches. There are certain problems of pressing practical concern for which it is not possible at present to make a reliable design prediction of high frequency vibration levels, as pointed out by Langley and Bardell (1998) recently. The present work introduces a novel numerical approach, the DSC algorithm, for the prediction of high frequency vibrations. The DSC algorithm has its theoretical foundation in mathematical distribution and wavelet analysis (Wei, 1999a, 2000a,b).

Rectangular plates having different combination of simply supported and clamped edges are studied in the present work. The computational philosophy of the DSC algorithm is briefly discussed and the formulation of the algorithm for plate analysis is given. Convergence studies are carried out for three selected square plates of various combinations of simply supported and clamped edges (SSSS, SSCS and CCCS). Numerical results are validated by the analytical solution for an SSSS plate and by the Levy solutions for SSCS and CSCS plates. The results showed that the DSC method is remarkably accurate for the SSSS plate. With a reasonable grid of 101^2 points, the first 2000 modes are accurate up to six decimal with relative errors less than 0.002%! Such results are firmly reliable for all practical purposes. In fact, the first 5000 modes, i.e., half of the modes computed by the DSC algorithm when the grid is 101^2, have less than 2% relative errors. What is of particular importance is that such a level of accuracy is also attained for SSCS and CSCS plates, as clearly verified by using the Levy method. Furthermore, the DSC results of the first

Table 4
Benchmark results for a wide range of frequency parameters for SCCS, CCCS, CCCC, SSCS and CSCS square plates

Mode number	SCCS	CCCS	CCCC	SSCS			CSCS		
				m, *n*	Levy	DSC	*m*, *n*	Levy	DSC
1	2.7412	3.2247	3.6461	1, 1	2.3959	2.3959	1, 1	2.9333	2.9333
2	6.1338	6.4168	7.4364	2, 1	5.2357	5.2357	2, 1	5.5466	5.5466
3	6.1589	7.2015	7.4364	1, 2	5.9421	5.9421	1, 2	7.0243	7.0243
4	9.4063	10.2124	10.9647	2, 2	8.7272	8.7273	2, 2	9.5835	9.5835
5	11.6070	11.7895	13.3320	3, 1	10.1594	10.1595	3, 1	10.3567	10.3567
6	11.6219	13.2074	13.3952	1, 3	11.4724	11.4724	1, 3	13.0801	13.0802
7	14.7707	15.3900	16.7182	3, 2	13.5559	13.5559	3, 2	14.2057	14.2057
8	14.8011	16.1584	16.7182	2, 3	14.2706	14.2707	2, 3	15.6821	15.6821
9	19.0951	19.2275	21.3305	4, 1	17.1191	17.1191	4, 1	17.2597	17.2597
10	19.1044	21.2091	21.3305	1, 4	18.9913	18.9914	3, 3	20.2450	20.2451
20	34.7391	36.2075	37.6257	4, 4	33.3929	33.3930	4, 4	34.9090	34.9093
30	48.3112	51.0975	51.7390	3, 6	47.6857	47.6860	7, 1	50.1407	50.1407
40	64.7455	66.3704	68.6682	6, 5	62.5471	62.5475	3, 7	64.5845	64.5857
50	77.2407	79.5953	81.6002	7, 5	75.3929	75.3934	7, 5	76.8786	76.8798
60	89.6319	94.1822	94.3854	2, 9	89.4308	89.4321	1, 9	91.1837	91.1863
70	106.0772	108.0343	111.2824	6, 8	103.1293	103.1308	4, 9	105.3301	05.3335
80	121.2973	122.0231	126.7117	10, 4	116.6969	116.6975	7, 8	118.9712	118.9749
90	133.4091	136.1961	138.9640	2, 11	130.4527	130.4554	5, 10	133.9991	134.0046
100	150.7732	152.9093	156.6604	11, 5	146.9699	146.9710	11, 5	147.9911	147.9934
200	282.0683	287.3487	290.2535	14, 9	279.2874	279.2935	14, 9	281.6552	281.6680
300	414.8046	421.2969	424.7275	19, 7	411.1180	411.1238	17, 11	415.6817	415.7090
400	549.6658	556.3167	561.4654	2, 23	544.5081	544.5547	22, 8	550.5552	550.5756
500	685.6417	688.2621	698.4053	23, 12	675.5755	675.6012	24, 10	679.5930	679.6311
600	813.5504	820.4249	827.2526	20, 20	806.7253	806.7981	21, 19	814.1774	814.3163
700	942.9947	951.1388	958.1161	26, 16	935.9042	935.9640	29, 10	944.0245	944.0762
800	1076.4061	1082.8963	1092.9462	24, 22	1067.0322	1067.1490	24, 22	1074.1757	1074.4087
900	1205.8808	1212.4433	1222.8903	32, 13	1195.2499	1195.3017	20, 28	1206.1283	1206.4169
1000	1331.9225	1344.5529	1349.9783	35, 10	1326.2558	1326.2901	23, 28	1333.8679	1334.3067
1100	1468.7253	1479.1107	1487.6199	17, 34	1459.8910	1460.1965	22, 31	1469.5310	1469.8863
1200	1595.3538	1606.5596	1614.9018	26, 30	1586.8300	1587.1250	26, 30	1597.7871	1598.3890
1300	1720.9126	1735.0494	1741.9705	35, 22	1714.4414	1714.6329	2, 41	1726.1888	1727.1385
1400	1865.3741	1870.1191	1886.9367	39, 18	1848.4722	1848.6140	23, 36	1854.5370	1855.6258
1500	1984.0690	1997.4696	2006.7157	4, 44	1973.9483	1974.5730	36, 26	1986.3091	1986.9106
1600	2119.8041	2130.4219	2142.7585	45, 9	2106.8029	2106.8461	22, 40	2118.3119	2119.5774
1700	2248.5308	2259.6464	2272.2598	38, 28	2235.7610	2236.1400	47, 6	2245.6948	2246.3819
1800	2373.6597	2388.1688	2398.4762	15, 46	2362.6586	2363.5258	11, 47	2375.7094	2377.1979
1900	2506.8575	2522.3544	2531.8733	13, 48	2496.0219	2497.0155	50, 2	2504.0730	2505.0099
2000	2635.1154	2648.3326	2661.3715	29, 42	2621.6734	2622.1712	51, 6	2637.6402	2637.7231
2100	2767.5094	2778.7656	2794.4360	38, 36	2751.6957	2752.4151	36, 38	2766.3235	2767.8171
2200	2900.0786	2912.6960	2927.3745	19, 50	2884.0555	2885.3089	51, 17	2894.9402	2895.3479
2300	3021.5580	3036.1981	3050.2438	53, 14	3006.6281	3007.8504	43, 34	3024.8493	3026.2351
2400	3158.9914	3170.2064	3188.1332	56, 2	3140.0323	3140.3602	20, 52	3151.9987	3152.6063
2500	3283.9973	3302.8475	3314.7279	48, 31	3272.8093	3273.4598	29, 49	3283.0935	3285.6637
2600	3415.1663	3428.3149	3445.5272	38, 44	3395.8811	3397.1408	48, 33	3410.4871	3412.0085
2700	3540.3785	3562.0715	3571.7963	4, 59	3526.4769	3529.8645	57, 17	3542.4532	3547.0979
2800	3670.2740	3684.9800	3703.3249	57, 20	3652.0248	3652.7695	32, 51	3666.9793	3671.0169
2900	3802.2018	3815.4974	3834.5337	57, 23	3781.9411	3782.7802	12, 60	3802.7913	3806.9741
3000	3927.0180	3946.0218	3960.6301	20, 59	3908.6293	3912.2589	62, 9	3926.1786	3930.6642
3100	4067.2403	4079.5244	4101.1149	56, 30	4042.5329	4044.3171	20, 60	4056.4468	4062.7810
3200	4187.1102	4205.7037	4223.7552	56, 32	4167.3359	4170.6384	35, 54	4184.9520	4190.8221
3300	4319.3183	4336.0908	4354.6685	63, 18	4295.2514	4300.2613	5, 65	4315.0084	4324.2689
3400	4454.3228	4469.8514	4490.3914	13, 65	4425.7692	4431.9106	40, 53	4449.7364	4455.4057

Table 4 (*continued*)

Mode number	SCCS	CCCS	CCCC	SSCS			CSCS		
				m, *n*	Levy	DSC	*m*, *n*	Levy	DSC
3500	4581.5446	4599.1441	4618.5821	67, 8	4553.4296	4559.1715	4, 67	4572.0996	4585.8606
3600	4715.8308	4733.9468	4753.5169	36, 58	4683.8663	4693.7048	26, 63	4702.4205	4714.7547
3700	4847.3230	4869.4905	4887.7473	61, 33	4817.2403	4830.0443	64, 27	4834.6587	4844.1591
3800	4981.7767	4995.6789	5023.4291	57, 41	4941.1539	4956.7979	69, 14	4959.5385	4978.4398
3900	5118.5513	5134.7453	5159.9795	45, 55	5070.3414	5093.7346	11, 70	5090.1831	5110.3664
4000	5248.5240	5268.6322	5288.5648	68, 24	5203.6459	5227.1931	72, 6	5220.4531	5245.0007
4100	5370.8915	5399.8919	5417.4298	71, 17	5331.7982	5354.7743	73, 4	5345.1989	5379.9032
4200	5507.1080	5533.3278	5553.5836	48, 56	5460.2679	5488.9994	68, 29	5475.4666	5515.5912
4300	5648.4529	5676.2094	5696.7488	73, 16	5586.5549	5627.2018	7, 74	5598.8349	5656.3552
4400	5791.3028	5811.2616	5838.2243	72, 23	5716.1890	5762.7119	73, 20	5733.8276	5785.6935
4500	5919.9068	5949.7340	5967.0847	22, 73	5847.6306	5903.4966	13, 75	5867.8656	5925.5958
4600	6067.8100	6090.7110	6114.4199	72, 28	5972.6389	6034.1115	75, 19	5990.2583	6064.0798
4700	6204.0308	6230.8582	6253.3629	78, 4	6100.0926	6180.9466	78, 6	6120.4181	6207.1339
4800	6349.6035	6370.5441	6401.9941	43, 66	6231.7122	6315.7984	79, 3	6250.1034	6340.5025
4900	6489.2809	6516.5479	6539.5444	62, 50	6358.6896	6464.9057	78, 17	6376.2990	6484.6309
5000	6632.9745	6661.4364	6695.0808	72, 36	6487.4019	6601.9842	31, 74	6504.2190	6633.3643

Here, m and n are the number of half waves in the y- and x-directions, respectively.

75% modes are all subject to less than 6% relative errors, which might not be very reliable, but might be still useful for predicting the trend of high frequency vibrations. Moreover, the DSC algorithm seems has no problem of numerical instability. Therefore, one can easily enlarge the DSC grid to achieve better convergence in a practical DSC prediction.

The frequency parameters of both the Levy method and the DSC algorithm are tabulated for SSCS and CSCS plates up to the first 5000 modes. The DSC algorithm is also used to provide frequency parameters for plates of SCCS, CCCS and CCCC edge supports. These results may serve as benchmark solutions for researchers to check their potential numerical methods for the analysis of high frequency vibrations.

Although this paper presents only high frequency vibration results for square plates with a few edge conditions, the DSC method is readily applied to rectangular plates with transversely supported edges, mixed support edges and with complex internal supports. The use of the method for the vibration analysis of plates with irregular geometries is under consideration. Moreover, many other DSC kernels, such as the regularized Dirichlet and Lagrange kernels, can be selected to give the high frequency analysis of the same level of confidence.

Acknowledgements

This work was supported by the National University of Singapore and by the University of Western Sydney.

References

Ablowitz, M.J., Herbst, B.M., Schober, C., 1996. On numerical solution of the sine-Gordon equation. J. Comput. Phys. 126, 299–314.

Banerjee, J.R., Williams, F.W., 1994. An exact dynamic stiffness matrix for coupled extensional–torsional vibrations of structural members. Comp. Struct. 50, 161–166.

Bardell, N.S., 1991. Free vibration analysis of a flat plate using the hierarchical finite element method. J. Sound Vib. 151, 263–289.

Beslin, O., Nicolas, J., 1997. A hierarchical functions set for predicting very high order plate bending modes with any boundary conditions. J. Sound Vib. 202, 633–655.
Guan, S., Lai, C.-H., Wei, G.W., 2001. Fourier–Bessel characterizations of patterns in a circular domain. Physica D 151, 83–98.
Keane, A.J., Price, W.G., 1987. Statistical energy analysis strongly coupled systems. J. Sound Vib. 117, 363–386.
Langley, R.S., Bardell, N.S., 1998. A review of current analysis capabilities applicable to the high frequency vibration prediction of aerospace structures. Aeronaut. J. 102, 287–297.
Langley, R.S., Khumbah, F.M., 1995. Prediction of high frequency vibration levels in built-up structures by using wave intensity analysis. 36th Structures, Structural Dynamics, and Material Conference, AIAA.
Lyon, R.H., 1975. Statistical Energy Analysis of Dynamical Systems: Theory and Applications. MIT Press, Cambridge, MA.
Mead, D.J., 1996. Wave propagation in continuous periodic structures: research contributions from Southampton. J. Sound Vib. 190, 495–524.
Mester, S.S., Benaroya, H., 1995. Periodic and near-periodic structures. Shock Vib. 2, 69–95.
Mindlin, R.D., 1951. Influence of rotatory inertia and shear on flexural motions of isotropic, elastic plates. Trans. ASME J. Appl. Mech. 18, 31–38.
Qian, L.W., Wei, G.W., A note on regularized Shannon's sampling formulae. J. Approx. Theor., submitted for publication.
Reddy, J.N., 1984. A simple higher-order theory for laminated composite plates. Trans. ASME J. Appl. Mech. 51, 745–752.
Schwartz, L., 1951. Théore des Distributions. Hermann, Paris.
Timoshenko, S.P., Woinowsky-Krieger, S., 1970. Theory of plates and shells. McGraw-Hill, Singapore.
Wan, D.C., Patnaik, B.S.V., Wei, G.W., 2001. Discrete singular convolution-finite subdomain method for the solution of incompressible viscous flows. J. Comput. Phys., in press.
Wang, T.M., Kinsman, T.A., 1971. Vibration of frame structures according to the Timoshenko theory. J. Sound Vib. 14, 215–227.
Wei, G.W., 1999a. Discrete singular convolution for the solution of the Fokker–Planck equations. J. Chem. Phys. 110, 8930–8942.
Wei, G.W., 1999b. Generalized Perona–Malik equation for image restoration. IEEE Signal Process. Lett. 6, 165–168.
Wei, G.W., 1999c. A unified method for computational mechanics. In: Wang, C.M., Lee, K.H., Ang, K.K. (Eds.), Computational Mechanics for the Next Millennium. Elsevier, Amsterdam, pp. 1049–1054.
Wei, G.W., 2000a. A unified approach for the solution of the Fokker–Planck equations. J. Phys. A, Math. Gen. 33, 4935–4953.
Wei, G.W., 2000b. Wavelet generated by using discrete singular convolution kernels. J. Phys. A, Math. Gen. 33, 8577–8596.
Wei, G.W., 2000c. Solving quantum eigenvalue problems by discrete singular convolution. J. Phys. B 33, 343–352.
Wei, G.W., 2000d. Discrete singular convolution method for the sine-Gordon equation. Physica D 137, 247–259.
Wei, G.W., 2001a. A new algorithm for solving some mechanical problems. Comput. Meth. Appl. Mech. Eng. 190, 2017–2030.
Wei, G.W., 2001b. Vibration analysis by discrete singular convolution. J. Sound Vib. 244, 535–553.
Wei, G.W., 2001c. Discrete singular convolution for beam analysis. Eng. Struct. 23, 1045–1053.
Wei, G.W., Zhao, Y.B., Xiang, Y. Discrete singular convolution and its application to the analysis of plates with internal supports. I. Theory and algorithm. Int. J. Numer. Meth. Eng., in press.
Xiang, Y., Liew, K.M., Kitipornchai, S., 1996. Exact buckling solutions for composite laminates: proper free edge conditions under in-plane loadings. Acta Mech. 117, 115–128.
Xiang, Y., Zhao, Y.B., Wei, G.W. Discrete singular convolution and its application to the analysis of plates with internal supports. II. Applications. Int. J. Numer. Meth. Eng., in press.
Zhao, Y.B., Xiang, Y., Wei, G.W. Plate vibration under irregular internal supports. Int. J. Solids Struct., in press.